Influence of Clay Content and Amount of Organic Modifiers on Morphology and Pervaporation Performance of EVA/Clay Nanocomposites

ARTICLE *in* INDUSTRIAL & ENGINEERING CHEMISTRY RESEARCH · FEBRUARY 2011

Impact Factor: 2.59 · DOI: 10.1021/ie102259s

I&EC research
Industrial & Engineering Chemistry Research

ARTICLE

pubs.acs.org/IECR

Influence of Clay Content and Amount of Organic Modifiers on Morphology and Pervaporation Performance of EVA/Clay Nanocomposites

Runcy Wilson,[†] Tomás S. Plivelic,[‡] P. Ramya,[§] C. Ranganathaiah,[§] M. Y. Kariduraganavar,[∥] Anil kumar Sivasankarapillai,[⊥,*] and Sabu Thomas

[†]School of Chemical Science, Mahatma Gandhi University, Kottayam, Kerala, 686560 India

[‡]MAX-lab, Lund University, SE 22100 Lund, Sweden

[§]Department of Studies in Physics, University of Mysore, Manasagangotri, 570 006 India

[∥]Center of Excellence in Polymer Science and Department of Chemistry, Karnataka University, Dharwad, India

[⊥]Department of Chemistry, N.S.S College, Ottapalam, Kerala, 679103 India

[¶]Center for Nano science and Nano technology, M.G University, P.D Hills, Kottayam, Kerala, 686560 India

ABSTRACT: Poly(ethylene-*co*-vinyl acetate)/organically modified clay nanocomposites were prepared using different clay loadings and by varying the amount of organic modifier. The morphology of the nanocomposites was investigated using small-angle X-ray scattering (SAXS), scanning electron microscopy (SEM), and transmission electron microscopy (TEM). SAXS results displayed intercalation of polymeric chains between the silicate layers in all the cases. The interlayer distance varies slightly between the series. TEM images showed a better dispersion of the clay platelets at lower loading for both series of samples. The pervaporation performances of membranes were analyzed using a chloroform/acetone mixture. Membranes displayed high selectivity. The influence of feed composition on pervaporation was analyzed. The nanoclay content and the influence of free volume on pervaporation performance were also investigated in detail. A drop in selectivity and an increase in permeation rate were observed at higher clay loadings.

INTRODUCTION

Polymer−clay nanocomposite is a new class of composite materials consisting of a polymer matrix with dispersed clay nanoparticles. Because of the unique characteristics of the nanometer size, dispersion of layered silicates with high aspect ratio, high surface area, and high strength in the polymer matrix, nanocomposite exhibits improvement in the properties compared with conventional micro- or macrocomposites. Polymer−clay nanocomposites were first synthesized by a Toyota research group in 1989 with a loading of 5% clay.[1,2] The clay particles can be dispersed in the matrix mainly in two forms: intercalated or exfoliated structures. Intercalated nanocomposites are formed when several polymer chains are inserted into the interlayer spaces to form a well-ordered alternating polymer/silicate layered nanostructure. Probably in this structure, the interlayer *d*-spacing could be expanded only to a limit of 20−80 Å. The exfoliated structure exhibits extensive penetration of the polymer and delamination of the layer structure. Exfoliation has an important goal in the preparation of polymer nanocomposites because this morphology is expected to produce a dramatic improvement in the stiffness, strength, dimensionless stability, flame retardancy, and reduction in the permeability of gases.[3]

Poly(ethylene-*co*-vinyl acetate) (EVA) has a wide range of applications such as electrical insulation, cable jacketing, component encapsulation, waterproofing, packaging of components, and the shoe industry, which directly highlights the extent of its industrial importance. Several studies were conducted on different properties of EVA/organically modified nanoclays such as rheology,[4] fire and thermal resistance,[5−9] and tensile testing.[10]

The improvement of these properties depends strongly upon the achieved degree of dispersion of the nanostructure in the polymer matrix. Peeterbroeck et al.[11] reported that the hydroxyl bearing ammonium cation that modifies the clay in Cloisite 30B increases the interaction between the acetate functions of EVA, which improved the mechanical and thermal properties of the nanocomposites. Ardhyananta et al.[12] showed that the presence of the ethylene glycol as a compatibilizer improves the processing properties, tensile strength, elongation at break, and thermal stability of the EVA/organoclay nanocomposites. These enhanced properties were due to the ionic interaction between the polymer chains and silicate surface.

Pervaporation is considered as a separation method in which a binary multicomponent liquid mixture is separated by partial vaporization through a dense nonporous membrane. During pervaporation, the feed mixture is in direct contact with one side of the membrane whereas permeate is removed as vapor from the opposite side into a vacuum or sweeping gas and then condensed.[13]

Received: September 13, 2010
Accepted: January 18, 2011
Published: February 24, 2011

dx.doi.org/10.1021/ie102259s | *Ind. Eng. Chem. Res.* 2011, 50, 3986–3993

Table 1. Descriptive Property of Nanoclays

nanoclays	organic modifier used	modifier concentration	d_{mc} (001) (Å)[a]
Cloisite 15A	dimethyl bis(hydrogenated tallow alkyl) quaternary ammonium cation.	95 mequiv/100 g of clay	28
Cloisite 20A	dimethyl bis(hydrogenated tallow alkyl) quaternary ammonium cation.	125 mequiv/100 gm of clay	24

[a] d_{mc} means *d*-value for the organo-modified clay previously reported in the literature.[27]

The driving force for the mass transfer of permeates from the feed side to the permeate side of the membrane is a gradient in chemical potential, which is established due to a difference in the partial pressures of permeate applied across the membrane.

Choudhari and Karidurganavar[14] prepared chitosan and Na^+-MMT clay membrane for the pervaporation of dehydration of isopropanol. Membranes with 10 wt % Na^+-MMT showed maximum selectivity. Susheel et al.[15] used sodium montmorillonite clay loaded polyvinyl alcohol membranes for the separation of aqueous mixtures of isopropanol and 1,4-dioxane. The modified membranes showed more selectivity toward the aqueous solution of isopropanol than to the aqueous solution of 1,4-dioxane. Wang et al.[16] investigated the effect of clay content on the pervaporation performance of 90 wt % aqueous ethanol solution through polyamide/clay nanocomposite membrane. They found that selectivity decreases sharply when the clay content gets higher than 2 wt %.

Dobarak et al.[17] reported that the incorporation of silicate filler increased the stability and selectivity of SBS-based membranes. Smuleac et al.[18] studied that the pervaporation of water/isopropanol mixture through perfluorinated polymer membrane showed a high selectivity for a broad range of feed concentration without swelling. Veeresh et al.[19] investigated that the extent of phosphomolybdic acid in the blend membranes of polyvinyl alcohol−poly(vinyl pyrrolidine) affected the pervaporation performance during ethanol dehydration. Picard and co-workers[20] studied the influence of clay dispersion on the transport properties of polyamide nanocomposites. In a previous work of our group, we had prepared EVA/clay nanocomposites with unmodified clay (Cloisite Na^+).[21] Pervaporation studies showed a far superior performance in solvent selectivity for the filled system compared to the unfilled one (Pure EVA).

In this study, poly(ethylene-*co*-vinyl acetate) (EVA) and two different organically modified nanoclay composites with varying clay loadings (3, 5, and 7 wt %) were prepared. The pervaporation characteristics of these films using chloroform−acetone mixtures were analyzed and then compared. Chloroform and acetone forms an azeotrope at 80 wt % of chloroform. Separation of azeotropes by simple distillation is possible only by adding a third component such as benzene, which is known to be a deadly carcinogen. Pervaporation is more effective in separating azeotropes. The morphology of nanocomposites was studied using scanning electron microscopy (SEM), transmission electron microscopy (TEM), and small-angle X-ray scattering (SAXS). The effect of free volume on the pervaporation performance was investigated by Positron Annihilation Life Time Spectroscopy (PALS).

2. EXPERIMENTAL SECTION

2.1. Materials. Poly(ethylene-*co*-vinyl acetate), EVA, with vinyl acetate content of 18 mol %, was obtained from Taisox Industries Limited, Taiwan. The cross-linking agent used was dicumyl peroxide (DCP). The nanoclays Cloisite 15A and Cloisite 20A were obtained from Southern Clay Products, United States. The descriptive properties of nanoclays are detailed in Table 1. The solvents, chloroform, and acetone used in the study were of reagent grade.

Table 2. Formulation of EVA/Clay Nanocomposites

			amount of nanoclay (kg)	
sample code	amount of EVA (kg)	amount of DCP (kg)	Cloisite 15A	Cloisite 20A
B_3	0.1	0.002	0.003	
B_5	0.1	0.002	0.005	
B_7	0.1	0.002	0.007	
C_3	0.1	0.002		0.003
C_5	0.1	0.002		0.005
C_7	0.1	0.002		0.007

2.2. Membrane Fabrication. Organically modified nanoclay-EVA membranes were prepared by melt mixing using dicumyl peroxide as the curing agent. The amount of the DCP used was 2 g. The mixing was done in a two roll mixing mill with a nip gap of 1.3 mm and at a friction ratio of 1:1.4. The nip gap, mill speed ratio, time of mixing, and temperature of the rolls were kept constant for all the mixes. The vulcanization behaviors of samples were studied by using a Monsanto Rheometer. The sheeted out samples were compression-molded in a hydraulic press at 160 °C under a load of 24.5×10^4 N .The samples were prepared with different clay content and designated as B_3, B_5, B_7, C_3, C_5, and C_7, where B and C represent the Cloisite 15A and Cloisite 20A organoclays, respectively. The formulations of the samples are given in Table 2.

2.3. Membrane Characterization. *2.3.1. Small-Angle X-ray Scattering.* The small-angle X-ray scattering (SAXS) experiments were carried out at I711 beamline of the MAX-lab Synchrotron, Sweden.[22] A monochromatic beam of 1.1 Å wavelength was used and the sample detector distance was 1245.47 mm for all the samples. Two-dimensional pictures were recorded using a 2D-CCD detector (165 mm active area from MAR Research, GmbH) with 10 min of data acquisition. Multilayer samples of 1 mm thickness were prepared by stacking pieces cut from a single film. The original orientation of the samples was preserved in the stack. The samples were placed in a multiple position sample holder and measured in an evacuated chamber.

X-ray scattering data were analyzed with the program FIT2D.[23] Average radial intensity profiles, $I(q)$, as a function of the scattering vector q ($q = 4\pi/\lambda \sin(\theta)$, where 2θ is the scattering angle and λ is the wavelength) were obtained by integrating the data in the complete image. For comparison of the scattering curves, the intensities were normalized by the integrated intensity incident on the sample during the exposure, and corrected by sample absorption, parasitic scattering, and background detector.

2.3.2. Scanning Electron Microscopy (SEM). The SEM micrographs of the polymer/clay nanocomposites were taken with a JEOL (Japan) model JSM 6390 electron microscope with an accelerating voltage of 10 kV.The specimens were prepared by cryogenically fracturing the vulcanized sheets in liquid nitrogen

and coating with platinum to avoid the electrostatic charge dissipation.

2.3.3. Transmission Electron Microscopy (TEM). The dispersion of layered silicates in polymer nanocomposites was investigated using the TEM analysis. Transmission electron micrographs of the nanocomposites were taken with a JEOL JEM 2100 transmission electron microscope with an accelerating voltage of 200 keV. Ultrathin sections of bulk specimens (~100 nm thickness) were obtained at −85 °C using an ultramicrotome fitted with a diamond knife.

2.3.4. Positron Annihilation Lifetime Spectroscopy (PALS). Positron annihilation lifetime spectroscopy is well-recognized as a powerful tool to conduce microstructural investigations of condensed matter. PALS was used to investigate the changes in the free volume of EVA/nanoclay composite membrane. The positron lifetime spectrometer used in the present study consists of a fast−fast coincidence system with BaF_2 scintillators coupled to photomultiplier tubes type XP2020/Q with quartz window as detectors. The detectors were shaped conical to achieve better time resolution. A 17 μCi ^{22}Na positron source deposited on a pure Kapton foil of 0.0127 mm thickness was placed between two identical pieces of samples under investigation. This sample-source sandwich was positioned between the two detectors of PALS to acquire lifetime spectrum. The spectrometer measures 180 ps as the resolution function with ^{60}Co source. However, for better count rate, the spectrometer was operated at 220 ps time resolution. All lifetime measurements were performed at room temperature and two to three positron lifetime spectra with more than a million counts under each spectrum were recorded. In PALS analysis for polymers and polymer-based composites mainly two parameters are of relevance, namely, *o*-Ps lifetime, τ_3, and *o*-Ps intensity, I_3 .The *o*-ps lifetime τ_3 measures the size of the free volume holes (V_f), and I_3 is a relative measure of the number of free volume sites in the polymer matrix.

2.4. Pervaporation. Pervaporation experiments were performed using an in-house designed apparatus.[24] In this setup, the permeation cell is assembled with two half cells of column couplers made of steel and fastened with bolted clamps. The capacity of the feed compartment was about 250 cm^3 and the effective surface area of the membrane in contact with the feed mixture was 34.23 cm^2. Vacuum at the downstream side was maintained by using a vacuum pump (Toshniwal, Chennai, India). A pressure of 2-3 mm of mercury was applied. Downstream pressure was measured with a vacuum gauge. The membrane was supported on a fine porous stainless steel plate. The membrane was kept in the pervaporation apparatus for about 1 h in each run to attain equilibrium conditions before collecting permeate. The permeate vapors were collected in a trap immersed in the liquid nitrogen jar on the downstream side . The flux was calculated by weighing permeate on a digital microbalance having an accuracy of ±0.01 mg. The feed and permeate compositions were analyzed by gas liquid chromatography. All experiments were carried out at 30 °C. The experiments were repeated three times and the results were averaged.

The performance of a given membrane in pervaporation is estimated in terms of its separation factor and permeate flux .The separation factor of the membrane can be estimated by the following equation,

$$\text{separation factor} = \frac{\frac{Y_i}{Y_j}}{\frac{X_i}{X_j}} \tag{1}$$

where Y_i and Y_j represent the weight fractions of chloroform and acetone in permeate and X_i and X_j represent those of chloroform and acetone in the feed, respectively.[21]

The flux can be calculated from the weight of the permeate collected after pervaporation using the following equation,[21]

$$J = \frac{Q}{A\,t} \tag{2}$$

where Q is the quantity in kilograms of permeate collected after a time (t) and A is the effective area of the membrane.[21]

Wijmans and Baker[25] derived an equation for pervaporation separation factor, β_{pervap}, which contains a term β_{evap} defined by the vapor−liquid equilibrium of the feed mixture and a term α_{mem}, the membrane selectivity, which is identical to the parameter in gas separation. An advantage of this method was that the role of operating conditions of pervaporation become clear. In our paper we have used this approach to calculate the intrinsic membrane properties. It can be seen that the overall selectivity is a combination of membrane selectivity and evaporative selectivity. Since the downstream pressure is negligible, the separation factor is given by

$$\beta_{pervap} = \beta_{evap}\alpha_{mem} \tag{3}$$

$$\alpha_{mem} = \frac{P_i}{P_j} \tag{4}$$

$$\beta_{evap} = \frac{p_i}{p_j}\frac{\gamma_i}{\gamma_j} \tag{5}$$

where P refers to the permeability and p and γ refer to vapor pressure and the activity coefficient of the components i and j, respectively.

Membrane selectivity is calculated using the equation

$$\alpha_{mem} = \frac{\beta_{pervap}}{\beta_{evap}} \tag{6}$$

2.5. Permeability, Permeance, and Selectivity. Pervaporation data in terms of fluxes and separation factors not only are a function of the intrinsic membrane properties but also depend on the operating conditions of the experiments. If we change the operating conditions such as temperature, feed concentration, and permeate pressure, all values will change. Baker et al.[26] established a new way of reporting pervaporation data in terms of permeability (P_i^G), permeance (P_i^G/l), and selectivity (α_{ij}).

Membrane permeability (P_i^G), a component flux normalized for membrane thickness, is given by the equation

$$P_j^i = j_i\frac{l}{P_{i0} - P_{il}} \tag{7}$$

where j_i is the molar flux, l is the thickness of the membrane, and P_{i0} and P_{il} are the vapor pressures of the component i on the feed and the permeate sides of the membrane, respectively.

Alternatively, when the membrane thickness is not known, membrane permeance (P_i^G/l), a component flux normalized for driving force, can be used.

$$\frac{P_i^G}{l}\frac{j_i}{p_{i0} - p_{il}} \tag{8}$$

Permeance is most commonly reported as gas permeation units (gpu) (1 gpu = 1×10^{-6} $cm^3(STP)/(cm^2\ scm\ Hg)$).

Membrane selectivity is defined as the ratio of the permeabilities or permeances of components i and j through the membrane.

$$\alpha_{ij} = \frac{P_i^G}{P_j^G} = \frac{\frac{P_i^G}{l}}{\frac{P_j^G}{l}} \quad (9)$$

3. RESULTS AND DISCUSSION

3.1. Small-Angle X-ray Scattering Analysis. It has been shown that the degree of delaminating of layered silicates and the distribution of interlayer distances in organo silicates can be determined from the SAXS data. This information is exceptionally useful for the analysis of nanocomposites because, qualitatively, it is possible to evaluate the affinity between the polymer chains and the organoclay based on the changes in SAXS profiles. For example, the shift of first maximum scattering toward a lower scattering vector can be attributed to the increase of interlayer distance caused by the intercalation of organoclay stacks by the polymer molecules. The widening of scattering peak and the decrease of the scattered intensity can be attributed to a beginning of exfoliation of organoclay stacks. The fully exfoliated clay will not show any interlayer peak but may show oscillations of a single-layer particle scattering.[27]

The small-angle X-ray scattering patterns of the polymer nanoclay composites B and C are shown in (a) and (b), respectively, of Figure 1. In all cases, the first peak indicated by an arrow can be associated with the lamellar periodicity produced by the semicrystalline character of the polymeric matrix. The other two peaks in each pattern present a significant intensity and is related to the intercalated polymer−organoclay structure. The d-spacing of the nanocomposites, d_N, obtained from the fitted position of the maximum (q_m) and using the relationship $d = 2\pi/q_m$ are reported in Table 3. To fit the experimental data, the addition of two Lorentzian functions and an exponential baseline was used in a restricted q range (from q values bigger than 0.1 $Å^{-1}$). The d-spacing of the two peaks follow a relationship 2:1, indicating that they are first- and second-order reflections of the same structure. Furthermore, all the values were far away for the reported values[27] of the pure organoclays Cloisite 15A and Cloisite 20A (d_{mc} see Table 1), confirming that the experimental peaks are due to the intercalation of polymers between organo-modified clay stacks.

We have reported earlier that the dispersion of non-organo-modified clay (Cloisite Na^+) in EVA is also characterized by the formation of intercalated morphology with increase in basal spacing compared to the pure clay.[21] Organo-modified clays in EVA (Cloisite15A and 20A, whose d-spacing differ substantially) exhibited intercalated morphology with a bigger increase in the interlayer spacing for all samples. Such a significant increase in the interlayer spacing indicates strong affinity of EVA chains with clay galleries. It is found that, in all the systems, interlayer spacing increases because of the intercalation of polymer into the layers of nanoclay.

In both sample series B and C, the clays were organically modified with the same surfactant, (dimethyl bis (hydrogenated tallow alkyl) ammonium cation) but differ in the amount of organic modifier. The interlayer spacing of the nanocomposites presents a slight dependence with the kind of organoclay and also on the content in the matrix. The highest value was obtained for the B series.

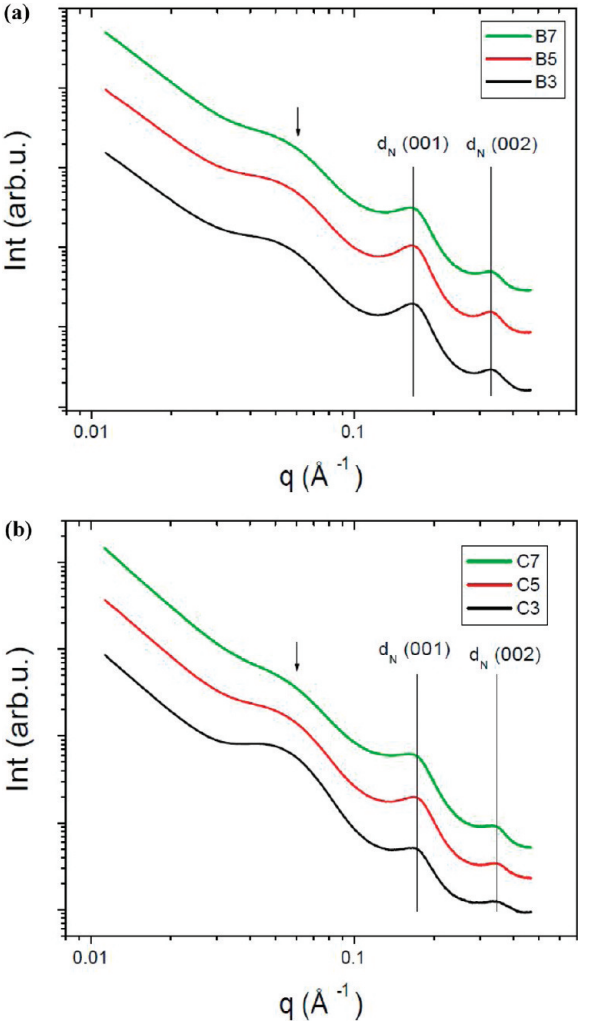

Figure 1. SAXS patterns of (a) EVA/organically modified Cloisite 15A nanocomposites and (b) EVA/organically modified Cloisite 20A nanocomposites. The solid lines indicate the peak maximum positions of the intercalated structure for B_3 and C_3 respectively. The curves are multiplied by an arbitrary scale factor to better visualize the sample's behavior.

Table 3. d-Spacing Values of Different Nanocomposites

series	sample	d_N (001) (Å)	d_N (002) (Å)
Cloisite 15A	B_3	36.58	18.53
	B_5	36.78	18.70
	B_7	36.76	18.71
Cloisite 20A	C_3	36.17	17.97
	C_5	35.80	17.96
	C_7	36.46	18.26

3.1.1. 2D SAXS Images. Orientation of the Intercalated Polymer/Clay Structures. The 2D SAXS patterns are useful in understanding the relative orientation of the silicate layers. The orientation of the different structures in the nanocomposites had special significance in its transport properties. Carretero-Gonzalez et al.[28] reported that the organically modified montmorillonite clays are more preferentially aligned than other organically modified clays like synthetic laponite or hectorite because of the large aspect ratio of the clay platelets.

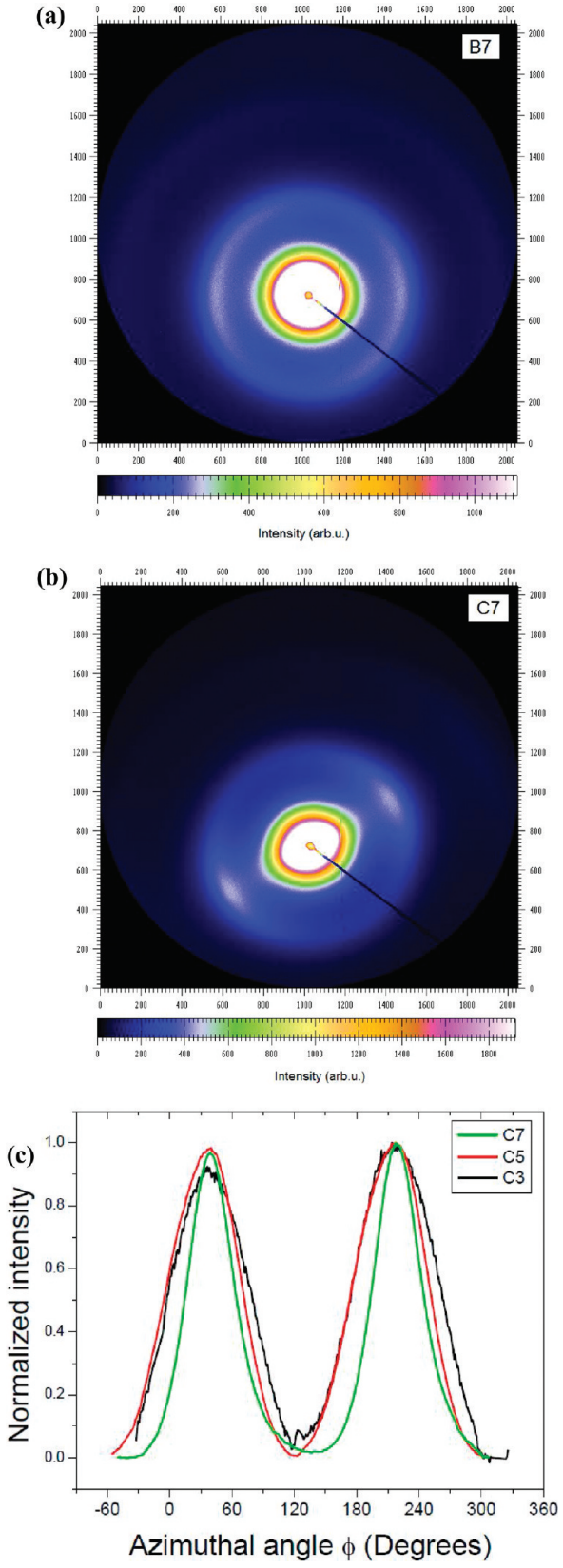

Figure 2. 2D SAXS images of nanocomposites. (a) EVA/clay nanocomposites of Cloisite15A clay with 7 wt % loading. (b) EVA/clay nanocomposites of Cloisite 20A clay with 7 wt % loading. (c) Azimuthal plot showing the orientation of intercalated polymer/clay structures in samples with Cloisite 20A clay (series C).

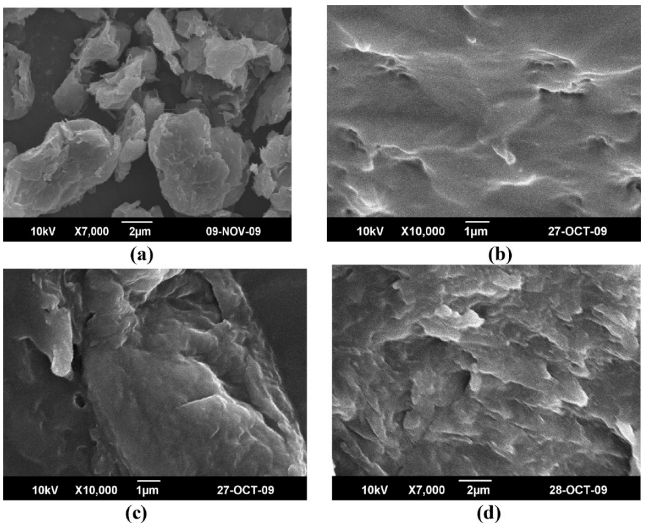

Figure 3. Scanning electron micrographs of EVA/clay nanocomposites. (a) SEM micrographs of Cloisite 20A. (b) SEM micrographs of EVA/Cloisite 20A nanocomposites with 3 wt % loading. (c) SEM micrographs of EVA/Cloisite 20A nanocomposites with 5 wt % loading. (d) SEM micrographs of EVA/Cloisite 20A nanocomposites with 7 wt % loading.

Figure 2 a,b presents the SAXS pictures for the highest clay concentration in both series, B_7 and C_7. In both cases, an anisotropic ring is noticed for the first-order reflection of intercalated polymer/clay stacking period. The nonuniform intensity in the ring indicated a preferential orientation of such periodic structures in the film plane.

The comparison of the anisotropy as a function of the clay content in the matrix is shown in Figure 2c for the series C, by using an azimuthal representation of the scattered intensity, $I(\varphi)$ vs φ (where $\varphi = 0$, when the scattering vector is at the equator and $\varphi = 90°$ at the meridian of the image; the data is averaged in the radial direction around the first-order reflection). Similar results were observed for B series. It is clear from Figure 2c that the full-width half maximum (fwhm) of the peaks decrease as a function of the clay concentration, indicating highly orientated intercalated structures for C_7 than C_3 or C_5. This effect (more oriented structures) can be a consequence of the formation of larger intercalated aggregates at higher clay contents.

3.2. Scanning Electron Microscopic Analysis. Scanning electron microscopic images of the Cloisite 20A and nanocomposites (series C) are shown in Figure 3a−c. Qualitatively, it can be seen that the surface morphology changes according to the clay loading and the particles appear to be better dispersed at lower clay loading. Smooth surfaces were found at lower clay loading and agglomerates of clay were observed at higher clay concentrations.

3.3. Transmission Electron Microscopic Analysis. TEM images provide the most direct visualization of the state of dispersion of clay particles in the nanocomposites. Figures 4 and 5 compares the morphology of nanocomposites of EVA with different loaded organically modified clays. The higher electron density of the silicates compared to EVA gives them a much darker appearance. The well-defined small and highly oriented clay stacks are responsible for the presence of defined peaks in SAXS data. TEM images show the homogeneous dispersion of individual silicate layers in the polymer matrix, but these stacks however lack a very good distribution within the polymer matrix at higher clay loadings and this result in the agglomeration of clay

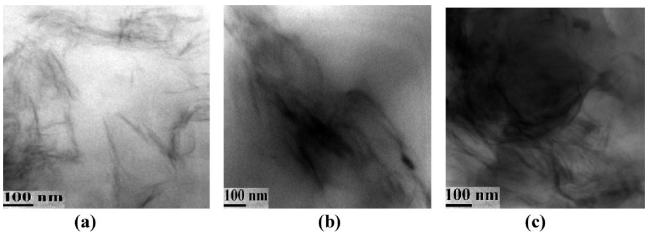

Figure 4. Transmission electron micrographs of EVA/clay nanocomposites. (a) TEM micrographs of EVA/Cloisite 15A nanocomposites with 3 wt % loading. (b) TEM micrographs of EVA/Cloisite 15A nanocomposites with 5 wt % loading. (c) TEM micrographs of EVA/Cloisite 15A nanocomposites with 7 wt % loading.

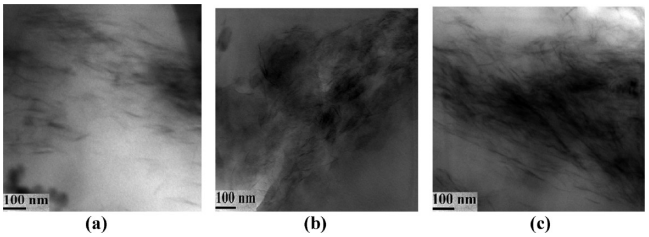

Figure 5. Transmission electron micrographs of EVA/clay nanocomposites. (a) TEM micrographs of EVA/Cloisite 20A nanocomposites with 3 wt % loading. (b) TEM micrographs of EVA/Cloisite 20A nanocomposites with 5 wt % loading. (c) TEM micrographs of EVA/Cloisite 20A nanocomposites with 7 wt % loading.

platelets. Best results are observed for Cloisite 15A and this sample is characterized by well-intercalated morphology consisting primarily of individually dispersed clay platelets. At higher clay loadings the image shows there is inhomogeneous dispersion of the individual silicate layers, which leads to partial exfoliation, intercalation, and agglomeration of the individual silicate layers.

Among the two series, the B series of nanocomposites provided a slightly better dispersion of clay platelets. When the percentage of clay increased, the dispersion decreased and the clay existed as agglomerates.

3.4. Positron Annihilation Lifetime Spectroscopy. The measurement of free volume in the context of the pervaporation process assumes an important role for understanding the performance of membrane and positron lifetime measurement directly provides this information. Positron annihilation technique has developed into a powerful characterization tool for the study of the free volume size and the free volume fraction in polymer material.

The influence of layered silicate on *o*-Ps lifetime, τ_3, *o*-Ps intensity, I_3, and relative fractional free volume percentage is presented in Table 4. It can be seen that the relative fractional free volume percentage was low for both samples at lower clay loading and increased monotonically with the clay contents. This can be attributed to the aggregation of clay layers for higher clay contents in the matrix, which resulted in additional void formation. This is also evident from the TEM images and SAXS results. Samples from series B showed slightly lower values of relative fractional free volume. Hence, it can be concluded that better clay dispersion is observed for sample B. In general, *o*-Ps annihilation lifetime (τ_3) mirrors size of free volume. An increase in *o*-Ps annihilation lifetime means an increase in free volume size. I_3 may not directly indicate the amount of free volume because the positron formation also depends on the decay rates and chemical environments.[29]

Table 4. PALS Measurement Data of Nanocomposites

sample	relative fractional free volume %	τ_3 (ns), *o*-Ps lifetime	I_3 (%), *o*-Ps intensity
B_3	5.37	2.51	20.84
B_5	5.70	2.52	21.84
B_7	5.85	2.56	21.40
C_3	5.56	2.53	19.81
C_5	5.87	2.53	21.23
C_7	5.92	2.55	21.31

Table 5. Pervaporation Characteristics of EVA/Clay Nanocomposites (22 wt % of Chloroform− Acetone Mixture)

sample	flux (kg/m^2·h)	separation factor α_{ij}
B_3	0.0398	62.12
C_3	0.0425	55.50
F_3[a]	0.12	36.0
EVA[a]	0.27	3.8

[a] Results taken from ref 21.

3.5. Pervaporation of Chloroform−Acetone Mixture. The pervaporation performance of the EVA/organo-modified clay nanocomposites were analyzed using the chloroform/acetone mixture (22 wt % of chloroform in the mixture). During the analysis it may be noted that the affinity of the EVA membrane toward chloroform is higher than acetone and this creates a remarkable difference in the separation of chloroform from chloroform/acetone mixtures.

The pervaporation characteristics of the different nanocomposites are tabulated in Table 5. In our earlier work it is shown that the EVA nanocomposites with unmodified clay showed a 10-fold increase in the separation factor compared to neat EVA membranes.[21] EVA nanocomposites with organo-modified clay showed a higher separation factor but a lower permeation rate compared to EVA nanocomposites with unmodified clay. The enhanced selectivity is due to the better nanometric dispersion of organic and inorganic phases. SAXS results showed better intercalation of polymer chains between the organically modified silicate layers for all samples. TEM images also showed better dispersion of clay platelets than the unmodified clay. Because of nanometric level dispersion of layered silicates, the contact area between the filler and the matrix increases, resulting in a reduced free volume and hence the separation factor increases. The platelets act as an impermeable barrier to the diffusing molecules, forcing them to follow a longer and more tortuous path to diffuse through the nanocomposites and this results in lower permeation rates.

3.6. Influence of Feed Composition. According to the solution-diffusion mechanism, permselective properties of pervaporation membranes are determined by solubility and diffusivity of the permeating components in the membrane. Since both sorption and diffusion phenomena are dependent on the composition of liquid mixture, the permeation properties are strongly influenced by the feed composition.

The effect of feed composition on the permeation rate and separation factor was investigated for B sample using different chloroform−acetone mixtures. Figure 6 represents the effect of

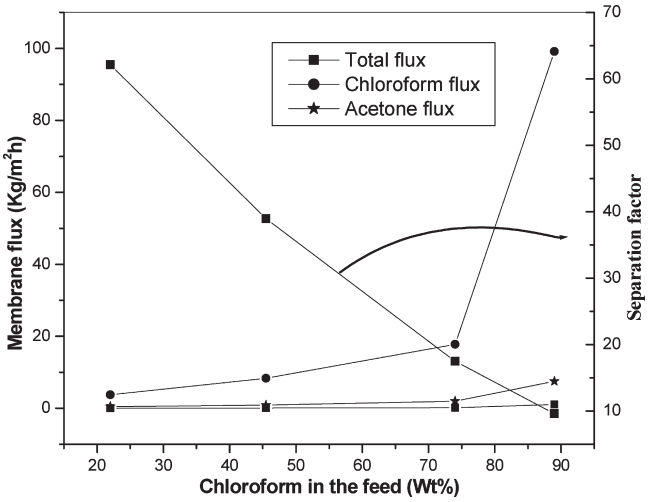

Figure 6. Influence of feed composition on pervaporation.

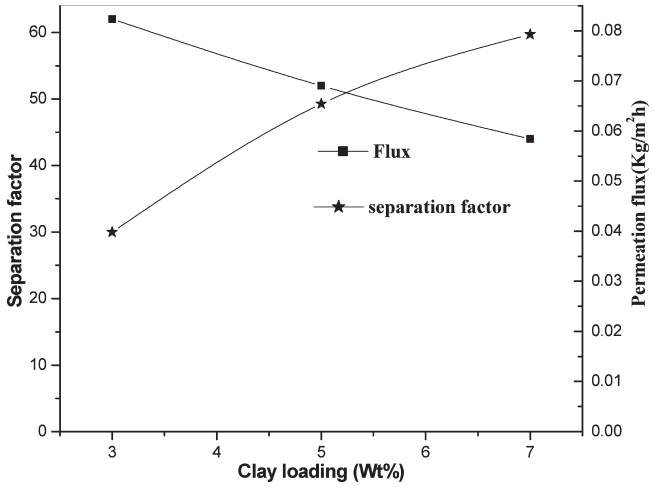

Figure 7. Influence of clay loading on the pervaporation performance for EVA/Cloisite 15A nanocomposites.

Table 6. Membrane Performance (22 wt % of Chloroform−Acetone Mixture)

sample	α_{mem}	β_{evap}
B	129.4	0.49
C	113.9	0.49

Table 7. Pervaporation Performance in Terms of Permeance and Selectivity

membrane	permeance (P/l) GPU	selectivity (α)
B	1080	4.5
C	1162	4

feed chloroform composition on total flux, component fluxes, and separation factor. At a low concentration of chloroform in the feed, the membrane is very selective and separation factor is high but the flux is low. As the concentration of chloroform in the feed is increased, flux increases and the separation factor falls. With the increase in chloroform content, the free volume of the membrane increases due to plasticization and this leads to higher flux.

When the chloroform concentration in the feed was higher, the amorphous region in the membranes became more swollen. Hence, the polymer chain in the swollen region became more flexible and the energy decreased for diffusive transport decreased, resulting in an increased permeation rate. Increased swelling at higher feed composition of chloroform has a negative impact on separation factor since the swollen and plasticized upstream membrane layer might have allowed some acetone molecules to escape into the permeate side, resulting in a reduced separation factor.

The membrane selectivity (α_{mem}) is calculated using eq 3. Table 6 gives the values for EVA/clay nanocomposites. It is found that the membrane selectivity is much higher than the evaporative selectivity. It is found that membrane selectivity overcomes the evaporative selectivity. The high value shows that the separation is not due to the evaporation of the feed liquid but by the membrane contribution. These values of membrane selectivity will provide an interesting study of how a mass-separating agent can overcome the intrinsic volatility differences and can enable a less volatile component in a mixture to be permeated. On the basis of these discussions, it is evident that the incorporation of organo-modified clay in EVA matrix produces highly selective membranes.

The influence of clay loading on pervaporation performance is presented in Figure 7. A composition of 22 wt % of chloroform/acetone mixture was used. The sample used is B. It is found that sample B has maximum separation factor at lower clay loading. A crucial factor that affects the permeation properties of the nanocomposites is the aggregation of nanoparticle at higher clay loading. These agglomerations may cause the formation of large-scale holes in the matrix. For high clay contents it is difficult to keep a high degree of platelet dispersion. TEM images show agglomeration of clay platelets at higher loading. Hence, a drop in selectivity and an increase in permeation rates were observed.

3.7. Permeance and Selectivity Values for EVA Membranes. The values of membrane permeance and selectivity for the pervaporation of chloroform−acetone mixture were calculated for two different types of membranes (B and C) and the values are presented in Table 7. Performance of a membrane depends on the value of selectivity. Membranes with no intrinsic membrane selectivity have selectivity value ≤ 1. Such a membrane would achieve the separation on simple evaporation of a portion of the liquid into the vapor phase. EVA/organically modified clay nanocomposites showed reasonably good selectivity and permeance value for chloroform−acetone mixture.

4. CONCLUSIONS

The influence of organically modified clay loading on the morphology and pervaporation performance of EVA/clay nanocomposites was studied. Samples with a varying amount of organic modifier (Cloisite 15A and Cloisite 20A) were also prepared. The morphology of the nanocomposites was evaluated using SAXS, transmission electron microscopy, and scanning electron microscopy. SAXS results showed intercalation of the polymeric chains between the silicate layers in all cases. First- and second-order reflection of the same structures were observed, indicating larger and well-ordered polymer/organoclay stacks. The interlayer spacing for the nanocomposite showed a slight dependence on the kind of organoclay and also the content of the

clay in the matrix. The higher spacing values were obtained for the B series with the larger amount of clay (B_5 and B_7).

TEM images showed a better dispersion of individual silicate layers at lower filler loading. At higher loadings, large aggregates were observed in close correlation with the SEM results. The trend of free volume size data in the polymer organically modified clay nanocomposites was evaluated by PALS. It can be seen that the relative fractional free volume percentage was low for both samples at lower clay loading and increased monotonically with the clay contents. Membranes based on organoclays showed superior performance in solvent selectivity than membranes with unmodified clays. The enhanced properties were due to the better interaction between organically modified silicate layers and polymer chains. It was observed that the membrane performance was strongly influenced by feed mixture composition. Pervaporation data in terms of permeance was also estimated and the value shows that separation is due to the membrane contribution.

AUTHOR INFORMATION

Corresponding Author

*E-mail: anugraha_anil@yahoo.co.in. Telephone: 09446045664. Fax: 91 481 2731002.

ACKNOWLEDGMENT

The authors are thankful to UGC, New Delhi, and KSCSTE, Trivandrum. SAXS data were collected at the 711 beamline of the MAX-lab synchrotron facility using beam time granted to T.S.P.

REFERENCES

(1) Uski, A.; Kojima, Y.; Kawasumi, M.; Okada, A.; Fujushima, A.; Kurauchi, T.; Kamigaito, O. Synthesis of nylon 6-clay hybrid. *J. Mater. Res.* **1993**, *8*, 1179.

(2) Kojima, Y.; Usuki, A.; Kawasumi, M.; Okada, A.; Fujushima, A.; Kurauchi, T.; Kamigaito, O. Mechanical properties of nylon 6-clay hybrid. *J. Mater. Res.* **1993**, *8*, 1185.

(3) Néel, J.; Noble, R. D.; Stern, S. A. *Pervaporation: Principles and Applications*; Elsevier: Amsterdam, 1995.

(4) Riva, A.; Zanetti, M.; Braglia, M.; Camino, G.; Falqui, L. Thermal degradation and rheoloical behaviour of EVA/montmorillonite nanocomposites. *Polym. Degrad. Stab.* **2002**, *77*, 299.

(5) Giannelli, W.; Camino, G.; Dintcheva, N. T.; LoVerso, S.; La Mantia, F. P. EVA-montmorillonite nanocomposites: Effect of processing conditions. *Macromol. Mater. Eng.* **2004**, *289*, 238.

(6) Alexandre, M.; Beyer, G.; Henrist, C.; Cloots, R.; Rulmont, A.; Jérôme, R.; Dubois, Ph. Preparation and Properties of Layered Silicate Nanocomposites Based on Ethylene Vinyl Acetate Copolymers. *Macromol. Rapid Commun.* **2001**, *22*, 643.

(7) Zanetti, M.; Camino, G.; Malhaupt, R. Combustion behaviour of EVA/fluorohectorite nanocomposites. *Polym. Degrad. Stab.* **2001**, *74*, 413.

(8) Hull, T. R.; Price, D.; Liu, Y.; Wills, C. L. Brady. An investigation into the decomposition and burning behaviour of Ethylene-vinyl acetate copolymer nanocomposite materials. *Polym. Degrad. Stab.* **2003**, *82*, 365.

(9) Duquesne, S.; Jama, C.; Le Bras, M.; Delobel., R.; Recourt, P.; Gloaguen, J. M. Elaboration of EVA−nanoclay systems—characterization, thermal behaviour and fire performance. *Compos. Sci. Technol.* **2003**, *63*, 1141.

(10) La Mantia, F. P.; Verso, S. L.; Dintcheva, N. T. EVA copolymer based nanocomposites. *Macromol. Mater. Eng.* **2002**, *287*, 909.

(11) Peeterbroeck, S.; Alexandre, M.; Jerome, R.; Dubois, Ph. Poly(ethylene-co-vinyl acetate)/clay nanocomposites: Effect of clay nature and organic modifiers on morphology, mechanical and thermal properties. *Polym. Degrad. Stab.* **2005**, *90*, 288.

(12) Ardhyananta, H.; Ismail, H.; Takeichi, T. Effects of organoclay loading and ethylene glycol on mechanical, morphology and thermal properties of ethylene vinyl acetate/organoclay nanocomposites. *J. Reinf. Plast. Compos.* **2007**, *26*, 789.

(13) Kujawski, W. Application of Pervaporation and Vapor Permeation in the Environmental Protection. *Polym. J. Environ. Stud.* **2000**, *9*, 13.

(14) Choudhari, S. K.; Karidurаganavar, M. Y. Development of novel composite membranes using quaternized chitosan and Na^+-MMT clay for the pervaporation dehydration of isopropanol. *J. Colloid Interface Sci.* **2009**, *338*, 111.

(15) Adoor, S. G.; Sairam, M.; Manjeshwa, L. S.; Raju, K. V. S. N.; Aminabhavi, T. M. Sodium montmorillonite clay loaded novel mixed matrix membranes of poly(vinyl alcohol) for pervaporation dehydration of aqueous mixtures of isopropanol and 1,4-dioxane. *J. Membr. Sci.* **2006**, *285*, 182.

(16) Wang, Y.C.; Fan, S.-C.; Lee, K.-R.; Li, C.-L.; Huang, S.-H.; Tsai, S.-H.; Lai, J.-Y. Polyamide/SDS−clay hybrid nanocomposite membrane application to water−ethanol mixture pervaporation separation. *J. Membr. Sci.* **2004**, *239*, 219.

(17) Dobrak, A.; Figoli, A.; Chovau, S.; Galiano, F.; Simore, S.; Vankelecom, I. F. J.; Drioli, E.; Van der Bruggen, B. Performance of PDMS membranes in pervaporation: Effect of silicalite fillers and comparison with SBS membranes. *J. Colloid Interface Sci.* **2010**, *346*, 254.

(18) Smuleac, V.; Wu, J.; Nemser, S.; Majumdar, S.; Battacharyya, D. Novel perfluorinated polymer-based pervaporation membranes for the separation of solvent/water mixtures. *J. Membr. Sci.* **2010**, *352*, 41.

(19) Magalad, T. V.; Siddappa, S. G.; Raju, K. V. S. N.; Aminabhavi, T. M. Mixed matrix blend membranes of poly(vinyl alcohol)−poly(vinyl pyrrolidone) loaded with phosphomolybdic acid used in pervaporation dehydration of ethanol. *J. Membr. Sci.* **2010**, *354*, 150.

(20) Picard, E.; Gérard, J. F.; Espuche, E. Water transport properties of polyamide 6 based nanocomposites prepared by melt blending: On the importance of the clay dispersion state on the water transport properties at high water activity. *J. Membr. Sci.* **2008**, *313*, 284.

(21) Anilkumar, S.; Kumaran, M. G.; Thomas, S. Characterization of EVA/clay nanocomposites membranes and its pervaporation performance. *J. Phys. Chem. B* **2008**, *112*, 4009.

(22) Knaapila, M.; Svensson, C.; Barauskas, J.; Zackrisson, M.; Nielsen, S. S.; Toft, K. N.; Vestergaard, B.; Arleth., L.; Olsson, U.; Pedersen, J. S.; Cerenius, Y. A new small-angle X-ray scattering set-up on the crystallography beamline I711 at MAX-lab. *J. Synchrotron Radiat.* **2009**, *16*, 498.

(23) Hammersley, A. P.; Svensson, S. O.; Thompson, A.; Graafsma, H.; Kvick, E.; Moy, J. P. Calibration and correction of distortions in two-dimensional detector systems. *Rev. Sci. Instrument.* **1995**, *66*, 2729.

(24) Muralidharan, M. N.; Anil Kumar, S.; Thomas, S. Pervaporation of alcohol-aromatic hydrocarbon mixtures through poly(ethylene-co-vinyl acetate) membranes. *J. Macromol. Sci.; Pure Appl. Chem.* **2009**, *46*, 274.

(25) Wijmans, J. G.; Baker, R. W. A simple predictive treatment of the permeation process in pervaporation. *J. Membr. Sci.* **1993**, *79*, 113.

(26) Baker, W. R.; Wijmans, J. G.; Huang, Y. Permeability, permeance and selectivity: A preferred way of reporting pervaporation performance data. *J. Membr. Sci.* **2010**, *348*, 346.

(27) Gelfer, M.; Burger, C.; Faddev, A.; Scis, I.; Chu, B.; Hsaio, B. S.; Henitz, A.; Kojo, K.; S-L, Hsu.; Si, M.; Rafailovich, M. Thermally induced phase transistions and morphological changes in organo clays. *Langmuir* **2004**, *20*, 3746.

(28) Carretero-Gonzalez, J.; Haris, R.; Raquel, V.; Shigeyuki, T.; Benjamin, S. H.; Emmanuel, P. G.; Miguel, A.; Lopez-Manchado. Effect of Nanoclay on Natural Rubber Microstructure. *Macromolecules* **2008**, *41*, 6763.

(29) Huang, S.-H.; Hung, W.-S.; Liaw, D.-J.; Li, C.-L.; Kao, S.-T.; Wang, D.-M.; De Guzman, M.; Hu, C.-C.; Jean, Y. C.; Lee, K.-R.; Lai, J.-Y. Investigation of multilayer pervaporation membrane by positrón annhilation spectroscopy. *Macromolecules* **2008**, *41*, 6438.